
FlightBench: A Comprehensive Benchmark of Spatial Planning Methods for Quadrotors

Shu-Ang Yu^{1*}, Chao Yu^{1*†}, Feng Gao^{1*}, Yi Wu^{1,2}, Yu Wang^{1†}
¹ Tsinghua University ² Shanghai Qi Zhi Institute

Abstract

Spatial planning in cluttered environments is crucial for mobile systems, particularly agile quadrotors. Existing methods, both optimization-based and learning-based, often focus only on success rates in specific environments and lack a unified platform with tasks of varying difficulty. To address this, we introduce FlightBench, the first comprehensive open-source benchmark for 3D spatial planning on quadrotors, comparing classical optimization-based methods with emerging learning-based approaches. We also develop a suite of task difficulty metrics and evaluation metrics to quantify the characteristics of tasks and the performance of planning algorithms. Extensive experiments demonstrate the significant advantages of learning-based methods for high-speed flight and real-time planning, while highlighting the need for improvements in complex conditions, such as navigating large corners or dealing with view occlusion. We also conduct analytical experiments to justify the effectiveness of our proposed metrics. Additionally, we show that latency randomization effectively enhances performance in real-world deployments. The source code is available at <https://github.com/thu-uav/FlightBench>.

1 Introduction

Collision-free spatial planning in cluttered environments is a fundamental capability for mobile systems and has been widely investigated [2, 5, 35, 40, 31]. It involves determining a collision-free path composed of multiple waypoints, derived from sensor data like cameras [1] and lidar [14]. A classical way to address the planning problem is through hierarchical methods, which separate it into distinct subtasks: mapping, path planning, and control [39]. In contrast, recent works [11, 12] have demonstrated that learning-based methods can unleash the full dynamic potential of agile platforms. These methods employ neural networks to directly map noisy sensory data to either mid-level collision-free trajectories [49] or low-level motion commands [31, 38]. Unlike the high computational costs associated with sequentially executed subtasks, this end-to-end mapping significantly reduces processing latency and enhances agility [16].

Despite the extensive investigation of diverse learning- and optimization-based planning methods, a unified benchmark for comparing these methods is still lacking. Existing planners are usually evaluated with customized scenarios and sensor configurations [24, 46, 29], thereby complicating the reproducibility of evaluations and hindering fair comparisons among different methods. Furthermore, there is also an absence of comprehensive and principled evaluation metrics that account for both task difficulty and planning performance. Some metrics, such as success rate, speed of the trajectory, and computation time, are widely used and straightforward for evaluating the performance of planners [16, 24]. However, these metrics are insufficient for accurately characterizing the quality of planning results.

*Equal Contributions

†Corresponding Authors. Chao Yu: zoe-yuchao@gmail.com, Yu Wang: yu-wang@tsinghua.edu.cn

Table 1: A comparison of FlightBench to other open-source planning benchmarks.

Benchmark	3D scenarios	Classical methods	Learning methods	Sensory input
MRBP 1.0 [37]	✗	✓	✗	LiDAR
Bench-MR [8]	✗	✓	✗	-
PathBench [32]	✓	✓	✓	-
Gibson Bench [38]	✗	✗	✓	Vision
OMPLBench [17]	✓	✓	✗	-
RLNav [42]	✗	✓	✓	LiDAR
FlightBench(Ours)	✓	✓	✓	Vision

Quadrotors, known for their agility and dynamism [34, 16], present unique challenges in integrating perception, planning, and control for safe flight. In this paper, we introduce FlightBench, a comprehensive benchmark that evaluates 3D spatial planning methods on quadrotors. We consider a suite of representative planners—two learning-based and three optimization-based—utilizing camera data and ground-truth state estimation. Additionally, we include two privileged planners with access to a global ground-truth map to serve as a superior criterion. We also propose novel task difficulty metrics to quantitatively assess the planning complexities of the three distinct scenarios introduced in FlightBench. Finally, we provide thorough performance metrics to compare different aspects of algorithmic effectiveness in planning. Our extensive experiments reveal the advantages and limitations of optimization-based and learning-based approaches regarding planning quality, flight speed, and computation time. Additionally, we analyze the effectiveness of the proposed metrics and emphasize the importance of latency randomization for learning-based methods. Key contributions are:

- The development of FlightBench, the first unified open-source benchmark that facilitates the comparison of learning-based and optimization-based spatial planning methods under various 3D scenarios.
- The proposition of tailored task difficulty and performance metrics for a comprehensive, quantitative evaluation of planning complexities and algorithmic performance.
- Detailed experimental analyses that demonstrate the comparative strengths and weaknesses of learning-based versus optimization-based planners, particularly under varied conditions.

2 Related Work

Spatial Planning Methods. Classical planning algorithms typically use search or sampling to explore the configuration or state space and generate a free path [10, 23, 20]. With optimization, a multi-objective optimization problem is often formulated to determine the optimal trajectory [19, 43]. This is commonly done using gradients from local maps, such as the Artificial Potential Field (APF) [48, 27] and the Euclidean Signed Distance Field (ESDF) [46]. On the other side, the development of deep learning enables algorithms to perform planning directly from sensory inputs such as images or lidar [39]. The policies are trained by imitating expert demonstrations [26] or through exploration under specific rewards [15]. Learning-based planners have been applied to various mobile systems, such as quadrupedal robots [1], wheeled vehicles [3, 31], and quadrotors [11, 41]. In this work, we examine representative spatial planners for quadrotors, including three optimization-based methods and two learning-based approaches, providing a comprehensive comparison between these categories.

Spatial Planning Benchmarks. Several benchmarks exist for non-sensor input planning algorithms, such as OMPL [17], Bench-MR [8], and PathBench [32]. OMPL and Bench-MR primarily focus on sampling-based planning methods, while PathBench evaluates graph-based and learning-based methods. For sensory input methods, most benchmarks are primarily designed for 2D scenarios. MRBP1.0 [37] and RLNav [42] evaluate planning methods with laser scan data to navigate around columns and cubes. GibsonBench [38] implements a mobile agent equipped with a camera, navigating in interactive environments. As outlined in Tab. 1, there’s still a lack of a benchmark with 3D scenarios and sensory inputs to assess and compare both classical and learning-based planning algorithms, which FlightBench aims to fill.

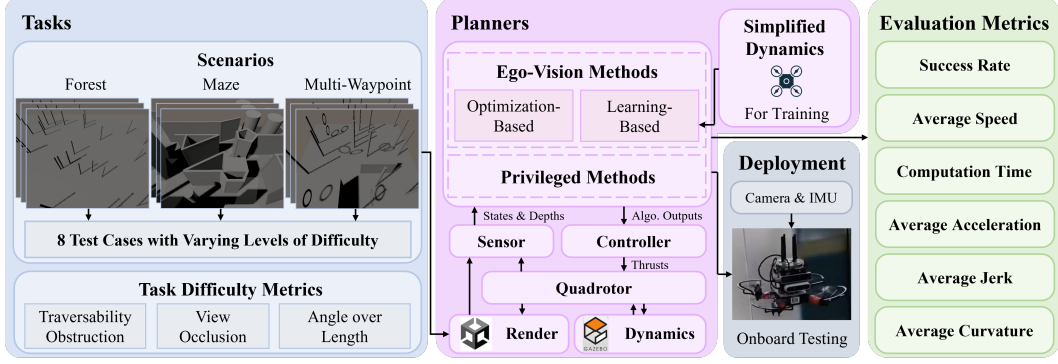


Figure 1: An overview of the FlightBench. FlightBench consists of three main components: (1) Tasks, featuring three scenarios categorized into eight difficulty levels. (2) Planners, the core benchmarking platform supporting five ego-vision planners and two privileged planners. (3) Evaluation Metrics, offering a thorough suite of performance assessment metrics.

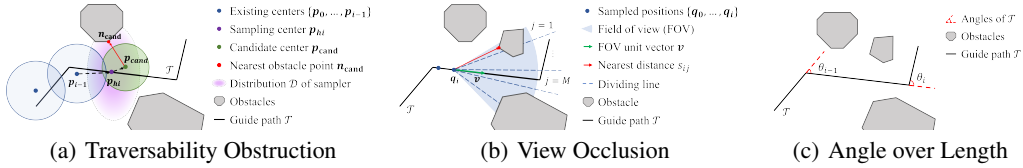


Figure 2: Illustration of the task difficulty metrics

3 FlightBench

In this section, we detail the components of FlightBench. An overview of our benchmark is depicted in Fig. 1. In FlightBench, to design a set of *Tasks* with distinguishable characteristics for comprehensive evaluation, we propose three difficulty metrics and develop eight test cases across three scenarios based on these metrics. We integrate various representative *Planners* to examine the strengths and features of both learning-based and optimization-based planning methods. Furthermore, we establish a comprehensive set of performance *Evaluation Metrics* to facilitate quantitative comparisons. Subsequent subsections will describe the Tasks, Planners, and Evaluation Metrics in depth.

3.1 Tasks

3.1.1 Task Difficulty Metrics

We utilize the topological guide path \mathcal{T} , which comprises interconnected individual waypoints [20], to characterize the planning difficulty of tasks. The task difficulty metrics consist of three aspects: *Traversability Obstruction* (TO), *View Occlusion* (VO), and *Angle Over Length* (AOL).

Traversability Obstruction. Traversability Obstruction (TO) measures the difficulty of spatial planning due to limited passable space caused by obstacles. We use a sampling-based approach [24] to construct sphere-shaped flight corridors $\{B_0, \dots, B_{N_T}\}$, where N_T is the number of spheres representing traversable space along path \mathcal{T} . Fig. 2(a) illustrates the computation of these corridors. The next sampling center \mathbf{p}_{hi} is chosen from existing spheres $\{B_0, \dots, B_{i-1}\}$ along \mathcal{T} . We sample K candidate centers from a 3D Gaussian distribution \mathcal{D} around \mathbf{p}_{hi} . Each candidate sphere B_{cand} is defined by its center \mathbf{p}_{cand} and radius $r_{cand} = \|\mathbf{p}_{cand} - \mathbf{n}_{cand}\|_2 - r_d$, where \mathbf{n}_{cand} is the nearest obstacle to \mathbf{p}_{cand} and r_d is the drone radius. For each B_{cand} , we calculate S_{cand} as $S_{cand} = k_1 V_{cand} + k_2 V_{inter} - k_3(\mathbf{d} \cdot \mathbf{z}) - k_4 \|\mathbf{d} - (\mathbf{d} \cdot \mathbf{z})\mathbf{z}\|_2$, where $k_1, k_2, k_3, k_4 \in \mathbb{R}^+$, V_{cand} is the volume of B_{cand} , V_{inter} is the overlap with B_{i-1} , $\mathbf{d} = \mathbf{p}_{cand} - \mathbf{p}_{hi}$, and \mathbf{z} is a unit vector along $\mathbf{p}_{hi} - \mathbf{p}_{i-1}$. The sphere B_{cand} with the highest S_{cand} is selected as the next sphere. This process continues until the entire path \mathcal{T} is covered. Since occlusion challenges mainly arise from the narrowest spaces, we order the

sphere radius $\{r_1, \dots, r_i, \dots, r_{N_T}\}$ in ascending order. The metric of traversability obstruction, \mathbb{T} , is defined as Eq. (1) where R represents the sensing range.

$$\mathbb{T} = \frac{1}{N_T} \sum_{i=1}^{\lfloor N_T/2 \rfloor} \frac{R}{r_i}. \quad (1)$$

View Occlusion. In online vision-input planning tasks, a narrow field of view (FOV) could hinder the drone’s perception [33, 4], thereby presenting a challenge to the perception-aware ability of planners [7]. We employ view occlusion (VO) to describe the occlusion impact of obstacles on the FOV within the scenario. The more obstructed the scenario, the higher the view occlusion. As shown in Fig. 2(b), we sample drone position $\{\mathbf{q}_i\}$ and FOV unit vector $\{\mathbf{v}_i\}$ along \mathcal{T} with $i \in \{1, \dots, N_V\}$. For each sampled pair $\{\mathbf{q}_i, \mathbf{v}_i\}$, we divide FOV into M parts and calculate the distance s_{ij} between the nearest obstacle point and drone position q_i in each part j . The view occlusion \mathbb{V} can be represented as Eq. (2), where m_j is a series of weights, which gives higher weight to obstacles closer to the center of the view.

$$\mathbb{V} = \frac{1}{N_V} \sum_{i=1}^{N_V} \sum_{j=1}^M m_j \frac{R}{s_{ij}}. \quad (2)$$

Angle Over Length. For a given scenario, frequent and violent turns in traversable paths pose challenges for the planner’s agility. Inspired by [8], we employ the concept of angle over length (AOL) denoted as \mathbb{A} to quantify the sharpness of a path. The AOL \mathbb{A} is defined by Eq. (3), where N_{AOL} signifies the number of angles depicted in Fig. 2(c), θ_i represents the i -th angle within the topological path \mathcal{T} , and L stands for the length of \mathcal{T} .

$$\mathbb{A} = \frac{1}{L} \sum_{i=1}^{N_{AOL}} \left(\exp \left(\frac{\theta_i}{\pi/6} \right) - 1 \right). \quad (3)$$

3.1.2 Scenarios and Tests

As illustrated in Fig. 1, our benchmark incorporates specific tests based on three scenarios: *Forest*, *Maze*, and *Multi-Waypoint*. These scenarios were chosen for their representativeness and frequent use in evaluating quadrotor planners [24, 11]. Within these scenarios, we developed eight tests, each characterized by varying levels of task complexity. The task difficulty scores for each test are detailed in Tab. 2.

The **Forest** scenario serves as a fundamental benchmark for quadrotor planners. We differentiate task difficulty based on obstacle density and establish three tests, following the settings of [16]. TO and VO metrics in the Forest scenario increase with higher tree density. AOL is particularly small due to the sparse obstacles, making this scenario suitable for high-speed flights [16, 24].

The **Maze** scenario consists of walls and boxes, creating consecutive sharp turns and narrow gaps. Quadrotors must navigate these confined spaces while maintaining flight stability and perception awareness [18]. We devise three tests with varying lengths and turn complexities for Maze, resulting in discriminating difficulty levels for VO and AOL.

The **Multi-Waypoint (MW)** scenario involves navigating through multiple waypoints at different heights sequentially [30]. This scenario also includes boxes and walls as obstacles. We have created two tests with different waypoint configurations. The MW scenario is relatively challenging, featuring the highest TO in test 1 and the highest AOL in test 2.

3.2 Planners

Here, we introduce the representative planning methods evaluated in FlightBench, covering three optimization-based planners, two learning-based planners, and two privileged methods with access to

Table 2: Task difficulty score of each test.

Scenario	Test	TO	VO	AOL
Forest	1	0.76	0.30	7.64×10^{-4}
	2	0.92	0.44	1.62×10^{-3}
	3	0.90	0.60	5.68×10^{-3}
Maze	1	1.42	0.51	1.36×10^{-3}
	2	1.51	1.01	0.010
	3	1.54	1.39	0.61
MW	1	1.81	0.55	0.08
	2	1.58	1.13	0.94

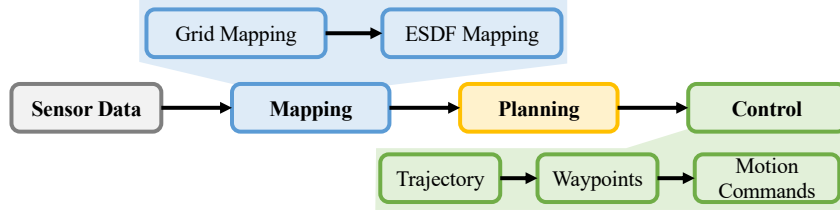


Figure 3: A generic processing pipeline for hierarchical spatial planners in quadrotors.

Table 3: Characteristics of the included Planners. "RL" denotes reinforcement learning, "IL" represents imitation learning, and "CTBR" stands for collective thrust and body rates. "GM" and "EM" refer to Grid Mapping and ESDF Mapping, respectively. The control level indicates the part of the control stack used by the planner.

	Method Type	Priv. Info.	Replan Horizon	Output	Mapping	Control Level
SBMT [20]	Samp.-based	✓	Long	Waypoints	✗	Middle
LMT [21]	RL	✓	-	CTBR	✗	Low
Fast-Planner [46]	Opti.-based	✗	Long	B-spline Traj.	GM+EM	High
EGO-Planner [47]	Opti.-based	✗	Short	B-spline Traj.	GM	High
TGK-Planner [44]	Opti.-based	✗	Long	B-spline Traj.	GM	High
Agile [16]	IL	✗	Short	Waypoints	✗	Middle
LPA [29]	RL+IL	✗	-	CTBR	✗	Low

environmental information. The characteristics of each method are detailed in Tab. 3. For links to the open-source code, key parameters, and implementation details, please refer to Appendix A.

Optimization-based Planners. Optimization-based methods generally consist of an online mapping module followed by a planning module. The three optimization-based planners described below generate B-spline trajectories (see Tab. 3). The control stack samples mid-level waypoints from the trajectory function and uses a low-level Model Predictive Control (MPC) controller to convert these waypoints into motor commands (Fig. 3). Among these planners, **Fast-Planner** [46] constructs both occupancy grid and Euclidean Signed Distance Field (ESDF) maps, whereas **TGK-Planner** [44] and **EGO-Planner** [47] only require an occupancy grid map. In the planning stage, **EGO-Planner** [47] focuses on trajectory sections with new obstacles, acting as a local planner, while the other two use a global search front-end and an optimization back-end for long-horizon planning.

Learning-based Planners. Utilizing techniques such as imitation learning (IL) and reinforcement learning (RL), learning-based planners train neural networks for planning, bypassing the time-consuming mapping process. **Agile** [16] employs DAGGER [25] to imitate an expert generating collision-free trajectories using Metropolis-Hastings sampling and outputs mid-level waypoints. **LPA** [29] combines IL and RL, starting with training a teacher policy using **LMT** [21], then distilling this expertise into a ego-vision student. Both teacher and student policies generate executable motion commands, specifically collective thrust and body rates (CTBR).

Privileged Planners. **SBMT** [20] is a sampling-based method that uses global ESDF maps to generate a collision-free trajectory of dense points, tracked by a perception-aware MPC (PAMPC) controller [6]. Its follow-up, **LMT** [21], employs RL to train an end-to-end policy for minimum-time flight. This policy uses the quadrotor's full states and the next collision-free point (CFP) to produce motion commands, with the CFP determined by finding the farthest collision-free point on a reference trajectory [20].

3.3 Evaluation Metrics

We represent quadrotor states as a tuple $(\mathbf{x}(t), \mathbf{v}(t), \mathbf{a}(t), \mathbf{j}(t))$, where t denotes time, $\mathbf{x}(t)$ denotes the position, and $\mathbf{v}(t) = \dot{\mathbf{x}}(t)$, $\mathbf{a}(t) = \dot{\mathbf{v}}(t)$, $\mathbf{j}(t) = \dot{\mathbf{a}}(t)$ are the velocity, acceleration, and jerk in the world frame, respectively. T denotes the time taken to fly from the starting point to the goal point.

First, we integrate three widely used metrics into FlightBench [24, 16]. **Success rate** measures if the quadrotor reaches the goal within a 1.5 m radius without crashing. **Average speed**, defined as $\frac{1}{T} \int_0^T \|\mathbf{v}(t)\|_2 dt$, reflects the achieved agility. **Computation time** evaluates real-time performance as the sum of processing times for mapping, planning, and control. Additionally, we introduce **average acceleration** and **average jerk** [46, 47], defined as $\bar{\mathbf{a}} = \frac{1}{L} \int_0^T \|\mathbf{a}(t)\|_2^2 dt$ and $\bar{\mathbf{j}} = \frac{1}{L} \int_0^T \|\mathbf{j}(t)\|_2^2 dt$, respectively. Average acceleration indicates energy consumption, while average jerk measures flight smoothness [36]. These metrics, though not commonly used in evaluations, are crucial for assessing practicability and safety in real-world applications. However, average acceleration and jerk only capture the dynamic characteristics of a flight. For instance, higher flight speeds along the same trajectory result in greater average acceleration and jerk. To assess the static quality of trajectories, we propose **average curvature**, inspired by [8]. Curvature is calculated as $\kappa(t) = \frac{|\mathbf{v}(t) \times \mathbf{a}(t)|}{|\mathbf{v}(t)|^3}$, and average curvature is defined as $\bar{\kappa} = \frac{1}{L} \int_0^T \kappa(t) \mathbf{v}(t) dt$.

Together, these six metrics provide a comprehensive assessment of quadrotor planner performance. Our extensive experiments will demonstrate that while learning-based methods excel in certain metrics, they also have shortcomings in others.

4 Experiments

Upon FlightBench, which provides a variety of metrics and scenarios to evaluate planner performance, we conduct extensive experiments to study the following research questions: (1) What are the main advantages and limitations of learning-based planners compared to optimization-based methods? (2) How does the planner’s performance vary across different scenario settings? (3) How much does the system latency introduced by the practical evaluation environment affect performance?

4.1 Setup

For simulating quadrotors, we use Flightmare [28] with Gazebo [13] as its dynamic engine. To mimic real-world conditions, we develop a simulated quadrotor model equipped with an IMU sensor and a depth camera, calibrated with real flight data. The physical characteristics of the quadrotor and sensors are detailed in Appendix B. To simulate real-world communication delays, all data transmission in the simulation uses ROS [22]. All simulations are conducted on a desktop PC with an Intel Core i9-11900K processor and an Nvidia 3090 GPU. To evaluate real-time planning performance on embedded platforms with limited computational resources, we also measure computation time on the Nvidia Jetson Orin NX module. Each evaluation metric is averaged over ten independent runs.

4.2 Benchmarking Planning Performance

4.2.1 Planning Quality

To systematically assess the strengths and weaknesses of various planning methods, we conduct evaluations across all tests within three distinct scenarios. Tab. 4 displays the results for the most challenging tests in each scenario. The comprehensive results for all tests are included in Appendix C.1 due to space limitations. We evaluate these methods using our proposed evaluation metrics, and computation time will be addressed separately in a subsequent discussion. In these experiments, we standardize the expected maximum speed at $3m/s$ for a fair comparison. Exceptions are SBMT, LMT, and LPA, whose flight speeds cannot be manually controlled.

As shown in Tab. 4, the privileged methods, with a global awareness of obstacles, set the upper bound for the planner’s motion performance in terms of average speed and success rate. In contrast, the success rate of ego-vision methods in the Maze and MW scenarios is generally below 0.6, indicating that our benchmark remains challenging for ego-vision methods, especially at the perception level.

Learning-based planners, known for their aggressive maneuvering, tend to fly less smoothly and consume more energy. They also experience more crashes in areas with large corners, as seen in the Maze and MW scenarios. When performing a large-angle turn, an aggressive planner is more likely to cause the quadrotor to lose balance and crash. Optimization-base methods are still competitive or even superior to current learning-based approaches, particularly in terms of minimizing energy costs. By contrasting the more effective Fast-Planner with the more severely impaired TGK-Planner and

Table 4: Performance evaluation of different planning methods under the most challenging test within each scenario. The highest performing values for each metric are highlighted in bold, with the second highest underlined.

Scen.	Metric	Privileged		Optimization-based			Learning-based	
		SBMT [20]	LMT [21]	TGK [44]	Fast [46]	EGO [47]	Agile [16]	LPA [29]
Forest	Success Rate \uparrow	0.80	1.00	<u>0.90</u>	<u>0.90</u>	1.00	<u>0.90</u>	1.00
	Avg. Spd. (ms^{-1}) \uparrow	15.25	<u>11.84</u>	2.30	2.47	2.49	3.058	8.96
	Avg. Curv. (m^{-1}) \downarrow	0.06	<u>0.07</u>	0.08	0.06	0.08	0.37	0.08
	Avg. Acc. (ms^{-3}) \downarrow	28.39	10.29	<u>0.25</u>	0.19	0.83	4.93	9.96
	Avg. Jerk (ms^{-5}) \downarrow	4.27×10^3	8.14×10^3	1.03	<u>3.97</u>	58.39	937.02	1.14×10^4
Maze	Success Rate \uparrow	<u>0.60</u>	0.9	0.50	<u>0.60</u>	0.20	0.50	0.30
	Avg. Spd. (ms^{-1}) \uparrow	<u>8.73</u>	9.62	1.85	1.99	2.19	3.00	8.35
	Avg. Curv. (m^{-1}) \downarrow	0.31	0.13	<u>0.17</u>	0.23	0.33	0.68	0.21
	Avg. Acc. (ms^{-3}) \downarrow	60.73	26.26	0.50	<u>0.79</u>	1.91	15.45	37.30
	Avg. Jerk (ms^{-5}) \downarrow	6.60×10^3	4.64×10^3	6.74	<u>9.62</u>	80.54	2.15×10^3	4.64×10^3
MW	Success Rate \uparrow	0.70	0.90	0.40	<u>0.80</u>	0.50	0.60	0.50
	Avg. Spd. (ms^{-1}) \uparrow	5.59	6.88	1.48	1.73	2.13	3.05	<u>6.72</u>
	Avg. Curv. (m^{-1}) \downarrow	0.47	<u>0.30</u>	0.46	0.32	0.62	0.67	0.26
	Avg. Acc. (ms^{-3}) \downarrow	80.95	31.23	<u>1.07</u>	0.97	5.06	16.86	36.77
	Avg. Jerk (ms^{-5}) \downarrow	9.76×10^3	1.66×10^4	<u>25.52</u>	22.72	155.83	2.07×10^3	6.19×10^3

EGO-Planner, we find that global trajectory smoothing and enhancing the speed of replanning are crucial for improving success rates in complex scenarios. Detailed analyses on the failure cases can be found in the Appendix C.2.

Remark. *Learning-based planners tend to execute aggressive and fluctuating maneuvers, yet they struggle with instability in scenarios with high challenges related to VO and AOL.*

4.2.2 Impact of Flight Speed

As discussed above, learning-based methods, which tend to fly more aggressively with greater fluctuation, underperform in scenarios requiring large turning angles. This section examines the performance of various methods in the expansive Forest scenario as flight speeds vary. We conduct experiments under test 2 of the Forest scenario, which records the highest TO values. As shown in Fig. 4, we evaluate the success rate of each method at different average flight speeds, excluding three methods where speed is integral to the planning process and non-adjustable.

Learning-based methods exhibit agile avoidance and operate closer to dynamic limits due to their straightforward end-to-end architecture. In contrast, optimization-based methods struggle in high-speed flights because their hierarchical architecture and latency between sequential modules can cause the quadrotor to overshoot obstacles before a new path is planned. A detailed analysis of the computation time for the pipeline is discussed in Sec. 4.2.3. Additionally, privileged planners show higher success rates and faster flights, highlighting the substantial potential for improvement in current ego-vision planners.

Remark. *Learning-based planners consistently surpass optimization-based baselines for high-speed flight, yet they fall significantly short of the optimal solution.*

4.2.3 Computation Time Analyses

To evaluate the computation time of various planning methods, we measured the time consumed at different stages on both desktop and onboard platforms. The results are presented in Tab. 5, with the computation time broken down into mapping, planning, and control stages as shown in Fig. 3. For learning-based methods, the mapping time includes converting images to tensors and pre-processing quadrotor states. Notably, SBMT optimizes the entire trajectory before execution, resulting in the highest computation time.

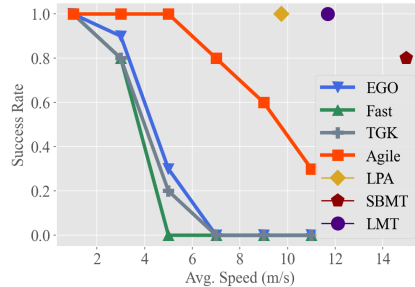


Figure 4: Success rate with different flight speeds.

Table 5: Computation time of different planners. T_{map} , T_{plan} , T_{ctrl} , T_{tot} stands for mapping time, planning time, control time, and total time, respectively.

		SBMT [20]	LMT [21]	TGK [44]	Fast [46]	EGO [47]	Agile [16]	LPA [29]
Desktop	T_{tot} (ms)	3.189×10^5	2.773	11.960	8.196	3.470	5.573	1.395
	T_{map} (ms)	-	1.607	3.964	7.038	2.956	0.338	0.399
	T_{plan} (ms)	2.589×10^5	1.167	7.994	1.155	0.510	5.115	0.995
	T_{ctrl} (ms)	-	-	0.002	0.003	0.003	0.119	-
Onboard	T_{tot} (ms)	-	13.213	37.646	39.177	24.946	27.458	12.293
	T_{map} (ms)	-	2.768	27.420	36.853	24.020	1.175	4.313
	T_{plan} (ms)	-	10.445	10.211	2.310	0.910	26.283	7.980
	T_{ctrl} (ms)	-	-	0.015	0.014	0.016	-	-

Table 6: Performance of RL-based methods under the hardest test of Multi-Waypoint scenario.

	Train w/ latency		Train w/o latency	
	Success Rate \uparrow	Progress	Success Rate \uparrow	Progress
LMT [21]	0.9	0.96	0.3	0.57
LPA [29]	0.5	0.73	0.0	0.32

The computation time for learning-based methods is significantly influenced by neural network design. Agile exhibits longer planning times compared to LPA and LMT due to its utilization of a MobileNet-V3 [9] encoder for processing depth images. Conversely, LPA and LMT employ simpler CNN and MLP structures, resulting in shorter inference time. Regarding optimization-based methods, the mapping stage often consumes the most time, particularly on the onboard platform. Fast-Planner experiences the longest mapping duration due to the necessity of constructing an ESDF map. EGO-Planner demonstrates superior planning time, even outperforming some end-to-end learning-based methods, owing to its local short-horizon replanning approach. Nonetheless, this may pose challenges in scenarios with high VO and AOL.

Remark. *Learning-based methods can achieve faster planning with compact neural network designs, while a well-crafted optimization-based planner can be equally competitive.*

4.3 Analyses on Effectiveness of Different Metrics

To demonstrate how various task difficulties influence different aspects of planning performance, we calculate the correlation coefficients between six performance metrics and three difficulty metrics for each method across multiple scenarios. The value at the intersection of the horizontal and vertical axes represents the absolute value of the correlation coefficient between the two metrics. A higher value indicates a stronger correlation. Fig. 5 presents the average correlations for privileged and ego-vision planners, separately evaluating the impacts on agility and partial observation. Refer to Appendix C.3 for calculation details and the specific correlation coefficients for each method.

The results for privileged planners shown in Fig. 5(a) indicate that AOL and TO have a significant impact on the planner’s motion performance. The correlation coefficients between AOL and average curvature, velocity and acceleration are all above 0.9, indicating that AOL describes the sharpness of the trajectory well. More specifically, high AOL results in high curvature and acceleration of the planned trajectory, as well as lower average speed. TO, indicating task narrowness, is a crucial determinant of flight success rates. In contrast to privileged methods where global information is accessible, as shown in Fig. 5(b), ego-vision planners primarily struggle with partial perception, where field-of-view occlusions and turns challenge real-time environmental awareness, making VO and AOL highly correlated with success rates.

Remark. *High VO and AOL significantly challenge learning-based planners, as these factors heavily impact the ego-vision method’s ability to handle partial observations and sudden reactions.*

4.4 Impact of Latency on Learning-based Methods

Beyond the algorithmic factors previously discussed, learning-based methods face considerable challenges transitioning from training simulations to real-world applications. Latency significantly

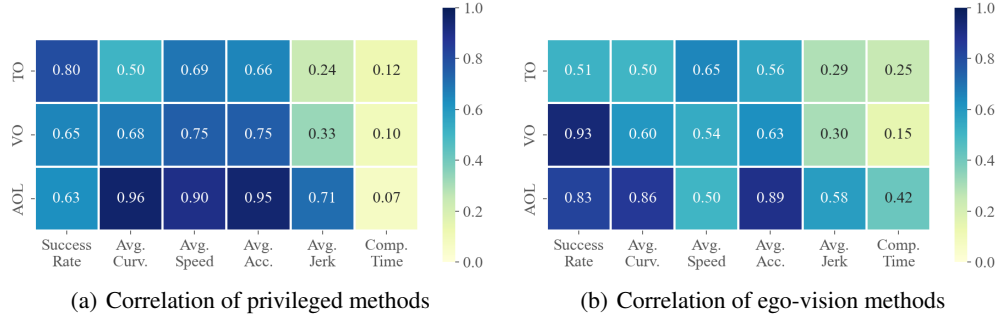


Figure 5: Correlation coefficients between three difficulty metrics and six evaluation metrics.

impacts sim-to-real transfer, particularly when simplified robot dynamics are used to enhance high-throughput RL training. We assess the influence of latency by testing learning-based planners in a ROS-based environment, where ROS, as an asynchronous system, introduces approximately $45ms$ of delay in node communication.

Tab. 6 details the performance of RL-based planners under the most challenging test, i.e., test 2 of the Multi-Waypoint scenario. To further evaluate a planner’s performance at low success rates, we introduce *Progress*, a metric ranging from 0 to 1 that reflects the proportion of the trajectory completed before a collision occurs. The “train w/ latency” column displays results from training with simulated and randomized latencies between $25ms$ to $50ms$, whereas the “train w/o latency” column serves as a control group. As shown in Tab. 6, “train w latency” significantly improves both success rate and progress by more than 50% for two methods, emphasizing the importance of incorporating randomized latency in more realistic simulation environments and real-world deployments.

Remark. *Integrating latency randomization into the training of RL-based methods is essential to enhance real-world applicability.*

5 Conclusion

In this work, we introduce FlightBench, a comprehensive open-source benchmark tailored for comparing learning-based and optimization-based methods for quadrotor spatial planning. FlightBench includes various representative planners and supporting modules, along with three task difficulty metrics and a thorough set of performance metrics. Our analysis reveals that while learning-based methods excel in high-speed flight, they require enhancements in trajectory smoothness and efficiency and are particularly affected by pipeline latency. For future work, we plan to expand FlightBench to cover broader domains, including multi-agent planning and dynamic obstacle avoidance. We believe our work will offer critical insights and provide challenging testbeds for advancing future learning-based planners.

References

- [1] Ananye Agarwal, Ashish Kumar, Jitendra Malik, and Deepak Pathak. Legged locomotion in challenging terrains using egocentric vision. In *Conference on robot learning*, pages 403–415. PMLR, 2023.
- [2] Malik Aqeel Anwar and Arijit Raychowdhury. Navren-rl: Learning to fly in real environment via end-to-end deep reinforcement learning using monocular images. In *2018 25th International Conference on Mechatronics and Machine Vision in Practice (M2VIP)*, pages 1–6. IEEE, 2018.
- [3] Devendra Singh Chaplot, Dhiraj Gandhi, Saurabh Gupta, Abhinav Gupta, and Ruslan Salakhutdinov. Learning to explore using active neural slam. *arXiv preprint arXiv:2004.05155*, 2020.
- [4] Xinyi Chen, Yichen Zhang, Boyu Zhou, and Shaojie Shen. Apace: Agile and perception-aware trajectory generation for quadrotor flights. *arXiv preprint arXiv:2403.08365*, 2024.
- [5] Wenzheng Chi, Chaoqun Wang, Jiankun Wang, and Max Q-H Meng. Risk-dtrrt-based optimal motion planning algorithm for mobile robots. *IEEE Transactions on Automation Science and Engineering*, 16(3):1271–1288, 2018.
- [6] Davide Falanga, Philipp Foehn, Peng Lu, and Davide Scaramuzza. Pampc: Perception-aware model predictive control for quadrotors. In *2018 IEEE/RSJ International Conference on Intelligent Robots and Systems (IROS)*, pages 1–8. IEEE, 2018.
- [7] Yuman Gao, Jialin Ji, Qianhao Wang, Rui Jin, Yi Lin, Zhimeng Shang, Yanjun Cao, Shaojie Shen, Chao Xu, and Fei Gao. Adaptive tracking and perching for quadrotor in dynamic scenarios. *IEEE Transactions on Robotics*, 2023.
- [8] Eric Heiden, Luigi Palmieri, Leonard Bruns, Kai O Arras, Gaurav S Sukhatme, and Sven Koenig. Bench-mr: A motion planning benchmark for wheeled mobile robots. *IEEE Robotics and Automation Letters*, 6(3):4536–4543, 2021.
- [9] Andrew Howard, Mark Sandler, Grace Chu, Liang-Chieh Chen, Bo Chen, Mingxing Tan, Weijun Wang, Yukun Zhu, Ruoming Pang, Vijay Vasudevan, et al. Searching for mobilenetv3. In *Proceedings of the IEEE/CVF international conference on computer vision*, pages 1314–1324, 2019.
- [10] Ishay Kamon and Ehud Rivlin. Sensory-based motion planning with global proofs. *IEEE transactions on Robotics and Automation*, 13(6):814–822, 1997.
- [11] Elia Kaufmann, Leonard Bauersfeld, Antonio Loquercio, Matthias Müller, Vladlen Koltun, and Davide Scaramuzza. Champion-level drone racing using deep reinforcement learning. *Nature*, 620(7976):982–987, 2023.
- [12] Elia Kaufmann, Antonio Loquercio, René Ranftl, Matthias Müller, Vladlen Koltun, and Davide Scaramuzza. Deep drone acrobatics. *arXiv preprint arXiv:2006.05768*, 2020.
- [13] N. Koenig and A. Howard. Design and use paradigms for gazebo, an open-source multi-robot simulator. In *2004 IEEE/RSJ International Conference on Intelligent Robots and Systems (IROS) (IEEE Cat. No.04CH37566)*, volume 3, pages 2149–2154 vol.3, 2004.
- [14] Fanze Kong, Wei Xu, Yixi Cai, and Fu Zhang. Avoiding dynamic small obstacles with onboard sensing and computation on aerial robots. *IEEE Robotics and Automation Letters*, 6(4):7869–7876, 2021.
- [15] Shiqi Liu, Mengdi Xu, Peide Huang, Xilun Zhang, Yongkang Liu, Kentaro Oguchi, and Ding Zhao. Continual vision-based reinforcement learning with group symmetries. In Jie Tan, Marc Toussaint, and Kourosh Darvish, editors, *Proceedings of The 7th Conference on Robot Learning*, volume 229 of *Proceedings of Machine Learning Research*, pages 222–240. PMLR, 06–09 Nov 2023.
- [16] Antonio Loquercio, Elia Kaufmann, René Ranftl, Matthias Müller, Vladlen Koltun, and Davide Scaramuzza. Learning high-speed flight in the wild. *Science Robotics*, 6(59):eabg5810, 2021.

- [17] Mark Moll, Ioan A Sucas, and Lydia E Kavraki. Benchmarking motion planning algorithms: An extensible infrastructure for analysis and visualization. *IEEE Robotics & Automation Magazine*, 22(3):96–102, 2015.
- [18] Jungwon Park, Yunwoo Lee, Inkyu Jang, and H Jin Kim. Dlsc: Distributed multi-agent trajectory planning in maze-like dynamic environments using linear safe corridor. *IEEE Transactions on Robotics*, 2023.
- [19] Liam Paull, Sajad Saeedi, Mae Seto, and Howard Li. Sensor-driven online coverage planning for autonomous underwater vehicles. *IEEE/ASME Transactions on Mechatronics*, 18(6):1827–1838, 2012.
- [20] Robert Penicka and Davide Scaramuzza. Minimum-time quadrotor waypoint flight in cluttered environments. *IEEE Robotics and Automation Letters*, 7(2):5719–5726, 2022.
- [21] Robert Penicka, Yunlong Song, Elia Kaufmann, and Davide Scaramuzza. Learning minimum-time flight in cluttered environments. *IEEE Robotics and Automation Letters*, 7(3):7209–7216, 2022.
- [22] Morgan Quigley, Ken Conley, Brian Gerkey, Josh Faust, Tully Foote, Jeremy Leibs, Rob Wheeler, Andrew Y Ng, et al. Ros: an open-source robot operating system. In *ICRA workshop on open source software*, volume 3, page 5. Kobe, Japan, 2009.
- [23] Stjepan Rajko and Steven M LaValle. A pursuit-evasion bug algorithm. In *Proceedings 2001 ICRA. IEEE International Conference on Robotics and Automation (Cat. No. 01CH37164)*, volume 2, pages 1954–1960. IEEE, 2001.
- [24] Yunfan Ren, Fangcheng Zhu, Wenyi Liu, Zhepei Wang, Yi Lin, Fei Gao, and Fu Zhang. Bubble planner: Planning high-speed smooth quadrotor trajectories using receding corridors. In *2022 IEEE/RSJ International Conference on Intelligent Robots and Systems (IROS)*, pages 6332–6339. IEEE, 2022.
- [25] Stéphane Ross, Geoffrey Gordon, and Drew Bagnell. A reduction of imitation learning and structured prediction to no-regret online learning. In *Proceedings of the fourteenth international conference on artificial intelligence and statistics*, pages 627–635. JMLR Workshop and Conference Proceedings, 2011.
- [26] Fabian Schilling, Julien Lecoœur, Fabrizio Schiano, and Dario Floreano. Learning vision-based flight in drone swarms by imitation. *IEEE Robotics and Automation Letters*, 4(4):4523–4530, 2019.
- [27] Joe Sfeir, Maarouf Saad, and Hamadou Saliyah-Hassane. An improved artificial potential field approach to real-time mobile robot path planning in an unknown environment. In *2011 IEEE international symposium on robotic and sensors environments (ROSE)*, pages 208–213. IEEE, 2011.
- [28] Yunlong Song, Selim Naji, Elia Kaufmann, Antonio Loquercio, and Davide Scaramuzza. Flightmare: A flexible quadrotor simulator. In *Proceedings of the 2020 Conference on Robot Learning*, pages 1147–1157, 2021.
- [29] Yunlong Song, Kexin Shi, Robert Penicka, and Davide Scaramuzza. Learning perception-aware agile flight in cluttered environments. In *2023 IEEE International Conference on Robotics and Automation (ICRA)*, pages 1989–1995. IEEE, 2023.
- [30] Yunlong Song, Mats Steinweg, Elia Kaufmann, and Davide Scaramuzza. Autonomous drone racing with deep reinforcement learning. In *2021 IEEE/RSJ International Conference on Intelligent Robots and Systems (IROS)*, pages 1205–1212. IEEE, 2021.
- [31] Kyle Stachowicz, Dhruv Shah, Arjun Bhorkar, Ilya Kostrikov, and Sergey Levine. Fastrlap: A system for learning high-speed driving via deep rl and autonomous practicing. In *Conference on Robot Learning*, pages 3100–3111. PMLR, 2023.

- [32] Alexandru-Iosif Toma, Hao-Ya Hsueh, Hussein Ali Jaafar, Riku Murai, Paul HJ Kelly, and Sajad Saeedi. Pathbench: A benchmarking platform for classical and learned path planning algorithms. In *2021 18th Conference on Robots and Vision (CRV)*, pages 79–86. IEEE, 2021.
- [33] Jesus Tordesillas and Jonathan P How. Panther: Perception-aware trajectory planner in dynamic environments. *IEEE Access*, 10:22662–22677, 2022.
- [34] Jon Verbeke and Joris De Schutter. Experimental maneuverability and agility quantification for rotary unmanned aerial vehicle. *International Journal of Micro Air Vehicles*, 10(1):3–11, 2018.
- [35] Jiankun Wang, Wenzheng Chi, Chenming Li, Chaoqun Wang, and Max Q-H Meng. Neural rrt*: Learning-based optimal path planning. *IEEE Transactions on Automation Science and Engineering*, 17(4):1748–1758, 2020.
- [36] Zhepei Wang, Xin Zhou, Chao Xu, and Fei Gao. Geometrically constrained trajectory optimization for multicopters. *IEEE Transactions on Robotics*, 38(5):3259–3278, 2022.
- [37] Jian Wen, Xuebo Zhang, Qingchen Bi, Zhangchao Pan, Yanghe Feng, Jing Yuan, and Yongchun Fang. Mrpb 1.0: A unified benchmark for the evaluation of mobile robot local planning approaches. In *2021 IEEE international conference on robotics and automation (ICRA)*, pages 8238–8244. IEEE, 2021.
- [38] Fei Xia, William B Shen, Chengshu Li, Priya Kasimbeg, Micael Edmond Tchampi, Alexander Toshev, Roberto Martín-Martín, and Silvio Savarese. Interactive gibbon benchmark: A benchmark for interactive navigation in cluttered environments. *IEEE Robotics and Automation Letters*, 5(2):713–720, 2020.
- [39] Jiaping Xiao, Rangya Zhang, Yuhang Zhang, and Mir Feroskhan. Vision-based learning for drones: A survey, 2024.
- [40] Xuesu Xiao, Joydeep Biswas, and Peter Stone. Learning inverse kinodynamics for accurate high-speed off-road navigation on unstructured terrain. *IEEE Robotics and Automation Letters*, 6(3):6054–6060, 2021.
- [41] Jiaxu Xing, Angel Romero, Leonard Bauersfeld, and Davide Scaramuzza. Bootstrapping reinforcement learning with imitation for vision-based agile flight. *arXiv preprint arXiv:2403.12203*, 2024.
- [42] Zifan Xu, Bo Liu, Xuesu Xiao, Anirudh Nair, and Peter Stone. Benchmarking reinforcement learning techniques for autonomous navigation. In *2023 IEEE International Conference on Robotics and Automation (ICRA)*, pages 9224–9230. IEEE, 2023.
- [43] Hongkai Ye, Neng Pan, Qianhao Wang, Chao Xu, and Fei Gao. Efficient sampling-based multirotors kinodynamic planning with fast regional optimization and post refining. In *2022 IEEE/RSJ International Conference on Intelligent Robots and Systems (IROS)*, pages 3356–3363. IEEE, 2022.
- [44] Hongkai Ye, Xin Zhou, Zhepei Wang, Chao Xu, Jian Chu, and Fei Gao. Tgk-planner: An efficient topology guided kinodynamic planner for autonomous quadrotors. *IEEE Robotics and Automation Letters*, 6(2):494–501, 2020.
- [45] Chao Yu, Akash Velu, Eugene Vinitsky, Jiaxuan Gao, Yu Wang, Alexandre Bayen, and Yi Wu. The surprising effectiveness of ppo in cooperative multi-agent games. *Advances in Neural Information Processing Systems*, 35:24611–24624, 2022.
- [46] Boyu Zhou, Fei Gao, Luqi Wang, Chuhao Liu, and Shaojie Shen. Robust and efficient quadrotor trajectory generation for fast autonomous flight. *IEEE Robotics and Automation Letters*, 4(4):3529–3536, 2019.
- [47] Xin Zhou, Zhepei Wang, Hongkai Ye, Chao Xu, and Fei Gao. Ego-planner: An esdf-free gradient-based local planner for quadrotors. *IEEE Robotics and Automation Letters*, 6(2):478–485, 2020.

- [48] Qidan Zhu, Yongjie Yan, and Zhuoyi Xing. Robot path planning based on artificial potential field approach with simulated annealing. In *Sixth international conference on intelligent systems design and applications*, volume 2, pages 622–627. IEEE, 2006.
- [49] Yuanshao Zhu, Yongchao Ye, Shiyao Zhang, Xiangyu Zhao, and James Yu. Difftraj: Generating gps trajectory with diffusion probabilistic model. *Advances in Neural Information Processing Systems*, 36, 2024.

A Implementation Details

In this section, we detail the implementation specifics of benchmarking planners in FlightBench, focusing particularly on methods without open-source code.

A.1 Optimization-based planners

Fast-Planner [46]¹, EGO-Planner [47]², and TGK-Planner [44]³ have all released open-source code. We integrate their open-source code into FlightBench and apply the same set of parameters for evaluation, as detailed in Tab. 7.

Table 7: Key parameters of the optimization-based methods.

	Parameter	Value	Parameter	Value
All	Max. Vel.	3.0 ms ⁻¹	Max. Acc.	6.0 ms ⁻²
	Obstacle Inflation	0.09	Depth Filter Tolerance	0.15m
	Map Resolution	0.1m		
Fast-Planner [46] EGO-Planner [47]	Max. Jerk	4.0 ms ⁻³	Planning Horizon	6.5 m
TGK-Planner [44]	krtr/rho	0.13 m	Replan Time	0.005 s

A.2 Learning-based planners

Agile [16]⁴ is an open-source learning-based planner. For each scenario, we finetune the policy from an open-source checkpoint using 100 rollouts before evaluation.

LPA [29] has not provided open-source code. Therefore, we reproduce the two stage training process based on their paper. The RL training stage involves adding a perception-aware reward to LMT [21] method, which will be introduced in Appendix A.3. At the IL stage, DAGger [25] is employed to distill the teacher’s experience into an ego-vision student. All our experiments on LPA and LMT use the same set of hyperparameters, as listed in Tab. 8.

A.3 Privileged planners

SBMT [20]⁵ is an open-source sampling-based trajectory planner. Retaining the parameters in their paper, we use SBMT package to generate topological guide path to calculate the task difficulty metrics, and employ PAMPC [6] to track the generated offline trajectories.

We reproduce LMT [21] from scratch based on the original paper, implementing the observation, action, reward function, and training techniques described in the paper. PPO [45] is used as the backbone algorithm, and its hyperparameters are listed in Tab. 8.

B Onboard Parameters

The overall system is implemented using ROS 1 Noetic Ninjemys. As mentioned in the main paper, we identify a quadrotor equipped with a depth camera and an IMU from real flight data. The physical characteristics of the quadrotor and its sensors are listed in Tab. 9.

¹<https://github.com/HKUST-Aerial-Robotics/Fast-Planner>

²<https://github.com/ZJU-FAST-Lab/ego-planner>

³<https://github.com/ZJU-FAST-Lab/TGK-Planner>

⁴https://github.com/uzh-rpg/agile_autonomy

⁵https://github.com/uzh-rpg/sb_min_time_quadrotor_planning

Table 8: Key hyperparameters used in RL and IL.

	Parameter	Value	Parameter	Value
RL [45]	Actor Lr	5e-4	Critic Lr	5e-4
	PPO Epoch	10	Batch Size	51200
	Max Grad. Norm.	8.0	Clip Ratio	0.2
	Entropy Coefficient	0.01		
IL [25]	Lr	2e-4	Training Interval	20
	Training Epoch	6	Max Episode	2000

Table 9: Parameters of the quadrotor and the sensors. ω_{xy} and ω_z refer to the angular velocity of roll, pitch, and yaw in the body frame of the quadrotor. ‘‘SRT’’ refers to single rotor thrust and ‘‘FOV’’ denotes the field of view.

	Parameter	Value	Parameter	Value
Quadrotor	Mass	1.0 kg	Max ω_{xy}	8.0 rad/s
	Moment of Inertia	[5.9, 6.0, 9.8] g m ²	Max. ω_z	3.0 rad/s
	Arm Length	0.125 m	Max SRT	0.1 N
	Torque Constant	0.0178 m	Min. SRT	5.0 N
Sensors	Depth Range	4.0 m	Depth FOV	90° × 75°
	Depth Frame Rate	30 Hz	IMU Rate	100 Hz

C Additional Results

C.1 Benchmarking Performance

The main paper analyzes the performance of the planners only on the most challenging tests in each scenario due to space limitations. The full evaluation results are provided in Tab. 10, Tab. 11, and Tab. 12, represented in the form of ‘‘mean(std)’’.

The results indicate that optimization-based methods excel in energy efficiency and trajectory smoothness. In contrast, learning-based approaches tend to adopt more aggressive maneuvers. Although this aggressiveness grants learning-based methods greater agility, it also raises the risk of losing balance in sharp turns.

C.2 Failure Cases

As discussed in Sec. 4.2, our benchmark remains challenging for ego-vision planning methods. In this section, we specifically examine the most demanding tests within the Maze and Multi-Waypoint scenarios to explore how scenarios with high VO and AOL cause failures for the planners.

As shown in Fig. 6(a), Test 3 in the Maze scenario has the highest VO among all tests. Before the quadrotor reaches waypoint 1, its field of view is obstructed by wall (A), making walls (B) and the target space (C) invisible. The sudden appearance of wall (B) often leads to collisions. Additionally, occlusions caused by walls (A) and (C) increase the likelihood of navigating to a local optimum, preventing effective planning towards the target space (C).

Fig. 6(b) illustrates a typical Multi-Waypoint scenario characterized by high VO, TO, and AOL. In this scenario, the quadrotor makes a sharp turn at waypoint 2 while navigating through the waypoints sequentially. The nearest obstacle, column (D), poses a significant challenge due to the need for sudden reactions. Additionally, wall (E), situated close to column (D), often leads to crashes for planners with limited real-time replanning capabilities.

Video illustrations of failure cases are provided in the supplementary material.

Table 10: Performance evaluation of different planning methods in Forest scenario.

Tests	Metric	Privileged		Optimization-based			Learning-based	
		SBMT [20]	LMT [21]	TGK [44]	Fast [46]	EGO [47]	Agile [16]	LPA [29]
1	Success Rate	0.90	1.00	1.00	1.00	1.00	1.00	1.00
	Avg. Spd. (ms^{-1})	17.90 (0.022)	12.10 (0.063)	2.329 (0.119)	2.065 (0.223)	2.492 (0.011)	3.081 (0.008)	11.55 (0.254)
	Avg. Curv. (m^{-1})	0.073 (0.011)	0.061 (0.002)	0.098 (0.026)	0.100 (0.019)	0.094 (0.010)	0.325 (0.013)	0.051 (0.094)
	Comp. Time (ms)	$2.477 (1.350) \times 10^5$	2.721 (0.127)	11.12 (1.723)	7.776 (0.259)	3.268 (0.130)	5.556 (0.136)	1.407 (0.036)
	Avg. Acc. (ms^{-3})	31.54 (0.663)	9.099 (0.321)	0.198 (0.070)	0.254 (0.054)	54.97 (0.199)	4.934 (0.385)	10.89 (0.412)
	Avg. Jerk (ms^{-5})	4644 (983.6)	6150 (189.2)	0.584 (0.216)	3.462 (1.370)	3.504 (24.048)	601.3 (48.63)	7134 (497.2)
2	Success Rate	0.80	1.00	1.00	1.00	1.00	1.00	1.00
	Avg. Spd. (ms^{-1})	14.99 (0.486)	11.68 (0.072)	2.300 (0.096)	2.672 (0.396)	2.484 (0.008)	3.059 (0.006)	9.737 (0.449)
	Avg. Curv. (m^{-1})	0.069 (0.004)	0.066 (0.001)	0.116 (0.028)	0.068 (0.035)	0.122 (0.006)	0.327 (0.025)	0.071 (0.038)
	Comp. Time (ms)	$2.366 (2.009) \times 10^5$	2.707 (0.079)	11.75 (1.800)	7.618 (0.220)	3.331 (0.035)	5.541 (0.173)	1.411 (0.036)
	Avg. Acc. (ms^{-3})	34.88 (1.224)	11.14 (0.296)	0.117 (0.084)	0.258 (0.148)	1.265 (0.178)	4.703 (0.876)	14.79 (0.564)
	Avg. Jerk (ms^{-5})	4176 (1654)	9294 (380.7)	0.497 (0.484)	4.017 (1.471)	83.96 (20.74)	751.8 (118.4)	11788 (803.5)
3	Success Rate	0.80	1.00	0.90	0.90	1.00	0.90	1.00
	Avg. Spd. (ms^{-1})	15.25 (2.002)	11.84 (0.015)	2.300 (0.100)	2.468 (0.232)	2.490 (0.006)	3.058 (0.008)	8.958 (0.544)
	Avg. Curv. (m^{-1})	0.065 (0.017)	0.075 (0.001)	0.078 (0.035)	0.059 (0.027)	0.082 (0.013)	0.367 (0.014)	0.080 (0.094)
	Comp. Time (ms)	$2.512 (0.985) \times 10^5$	2.792 (0.168)	11.54 (1.807)	7.312 (0.358)	3.268 (0.188)	5.614 (0.121)	1.394 (0.039)
	Avg. Acc. (ms^{-3})	28.39 (3.497)	10.29 (0.103)	0.249 (0.096)	0.192 (0.119)	0.825 (0.227)	4.928 (0.346)	9.962 (0.593)
	Avg. Jerk (ms^{-5})	4270 (1378)	8141 (133.2)	1.030 (0.609)	3.978 (1.323)	58.395 (15.647)	937.0 (239.2)	11352 (693.6)

Table 11: Performance evaluation of different planning methods in Maze scenario.

Tests	Metric	Privileged		Optimization-based			Learning-based	
		SBMT [20]	LMT [21]	TGK [44]	Fast [46]	EGO [47]	Agile [16]	LPA [29]
1	Success Rate \uparrow	0.80	1.00	0.90	1.00	0.90	1.00	0.80
	Avg. Spd. (ms^{-1}) \uparrow	13.66 (1.304)	10.78 (0.056)	2.251 (0.123)	2.097 (0.336)	2.022 (0.010)	3.031 (0.004)	5.390 (0.394)
	Avg. Curv. (m^{-1}) \downarrow	0.087 (0.025)	0.079 (0.002)	0.154 (0.049)	0.113 (0.029)	0.179 (0.011)	0.135 (0.010)	0.252 (0.084)
	Comp. Time (ms) \downarrow	$1.945 (0.724) \times 10^5$	2.800 (0.146)	11.76 (0.689)	7.394 (0.475)	3.053 (0.035)	5.535 (0.140)	1.369 (0.033)
	Avg. Acc. (ms^{-3}) \downarrow	34.57 (6.858)	13.26 (0.374)	0.277 (0.161)	0.392 (0.223)	1.599 (0.220)	1.023 (0.128)	18.17 (0.708)
2	Avg. Jerk (ms^{-5}) \downarrow	4686 (1676)	10785 (149.1)	0.809 (0.756)	3.716 (1.592)	109.2 (25.81)	65.94 (15.66)	8885 (206.4)
	Success Rate \uparrow	0.70	1.00	0.80	0.90	0.60	0.70	0.80
	Avg. Spd. (ms^{-1}) \uparrow	13.67 (0.580)	10.57 (0.073)	2.000 (0.065)	2.055 (0.227)	2.022 (0.001)	3.052 (0.003)	9.314 (0.168)
	Avg. Curv. (m^{-1}) \downarrow	0.082 (0.009)	0.088 (0.002)	0.157 (0.053)	0.090 (0.026)	0.109 (0.002)	0.193 (0.009)	0.076 (0.081)
	Comp. Time (ms) \downarrow	$2.188 (1.160) \times 10^5$	3.047 (0.196)	11.58 (0.514)	7.557 (0.283)	2.997 (0.022)	5.579 (0.102)	1.371 (0.037)
3	Avg. Acc. (ms^{-3}) \downarrow	31.68 (1.443)	15.99 (0.274)	0.252 (0.102)	0.278 (0.084)	1.090 (0.147)	1.772 (0.336)	10.89 (0.531)
	Avg. Jerk (ms^{-5}) \downarrow	2865 (566.8)	8486 (392.6)	0.967 (0.759)	3.999 (1.015)	103.2 (18.75)	171.4 (30.66)	2062 (190.4)
	Success Rate \uparrow	0.60	0.90	0.50	0.60	0.20	0.50	0.50
	Avg. Spd. (ms^{-1}) \uparrow	8.727 (0.168)	9.616 (0.112)	1.849 (0.120)	1.991 (0.134)	2.189 (0.167)	2.996 (0.012)	8.350 (0.286)
	Avg. Curv. (m^{-1}) \downarrow	0.313 (0.034)	0.134 (0.008)	0.168 (0.060)	0.229 (0.057)	0.332 (0.020)	0.682 (0.084)	0.214 (0.093)
3	Comp. Time (ms) \downarrow	$1.649 (1.539) \times 10^5$	2.639 (0.100)	10.29 (0.614)	8.918 (0.427)	3.552 (0.111)	5.469 (0.081)	1.422 (0.037)
	Avg. Acc. (ms^{-3}) \downarrow	60.73 (5.686)	26.26 (1.680)	0.500 (0.096)	0.786 (0.306)	1.910 (0.169)	15.45 (3.368)	37.30 (1.210)
	Avg. Jerk (ms^{-5}) \downarrow	6602 (685.1)	4649 (305.8)	6.740 (0.226)	9.615 (4.517)	80.54 (7.024)	2151 (470.2)	4638 (428.4)

Table 12: Performance evaluation of different planning methods in Multi-Waypoint scenario.

Tests	Metric	Privileged		Optimization-based			Learning-based	
		SBMT [20]	LMT [21]	TGK [44]	Fast [46]	EGO [47]	Agile [16]	LPA [29]
1	Success Rate \uparrow	0.60	0.90	0.90	1.00	1.00	1.00	0.80
	Avg. Spd. (ms^{-1}) \uparrow	10.13 (0.343)	11.06 (0.107)	1.723 (0.075)	2.164 (0.140)	2.512 (0.017)	3.017 (0.029)	8.216 (1.459)
	Avg. Curv. (m^{-1}) \downarrow	0.177 (0.027)	0.087 (0.004)	0.119 (0.045)	0.118 (0.017)	0.159 (0.012)	0.406 (0.048)	0.223 (0.035)
	Comp. Time (ms) \downarrow	$1.199 (0.371) \times 10^5$	2.834 (0.163)	15.32 (0.684)	9.265 (0.542)	3.464 (8.786)	5.610 (0.161)	1.393 (0.035)
	Avg. Acc. (ms^{-3}) \downarrow	46.98 (10.46)	19.67 (1.300)	0.540 (0.080)	0.533 (0.169)	1.063 (0.173)	7.456 (1.249)	34.00 (1.551)
	Avg. Jerk (ms^{-5}) \downarrow	5051 (865.4)	5641 (358.0)	6.287 (0.899)	12.03 (4.145)	64.50 (12.90)	1378 (776.3)	9258 (2238)
2	Success Rate \uparrow	0.70	0.90	0.40	0.80	0.50	0.60	0.50
	Avg. Spd. (ms^{-1}) \uparrow	5.587 (1.351)	6.880 (0.366)	1.481 (0.092)	1.735 (0.241)	2.132 (0.339)	3.053 (0.034)	6.721 (0.980)
	Avg. Curv. (m^{-1}) \downarrow	0.469 (0.029)	0.296 (0.031)	0.463 (0.046)	0.320 (0.047)	0.617 (0.216)	0.668 (0.056)	0.263 (0.051)
	Comp. Time (ms) \downarrow	$6.437 (0.250) \times 10^5$	2.649 (0.185)	12.32 (2.042)	9.725 (0.818)	4.584 (0.734)	5.683 (0.140)	1.390 (0.039)
	Avg. Acc. (ms^{-3}) \downarrow	80.95 (15.10)	31.23 (1.213)	1.067 (0.083)	0.972 (0.470)	5.060 (1.523)	16.86 (1.422)	36.77 (10.36)
	Avg. Jerk (ms^{-5}) \downarrow	9760 (1000)	16565 (3269)	25.52 (7.914)	22.72 (11.14)	155.8 (114.1)	2070 (551.0)	6187 (956.2)

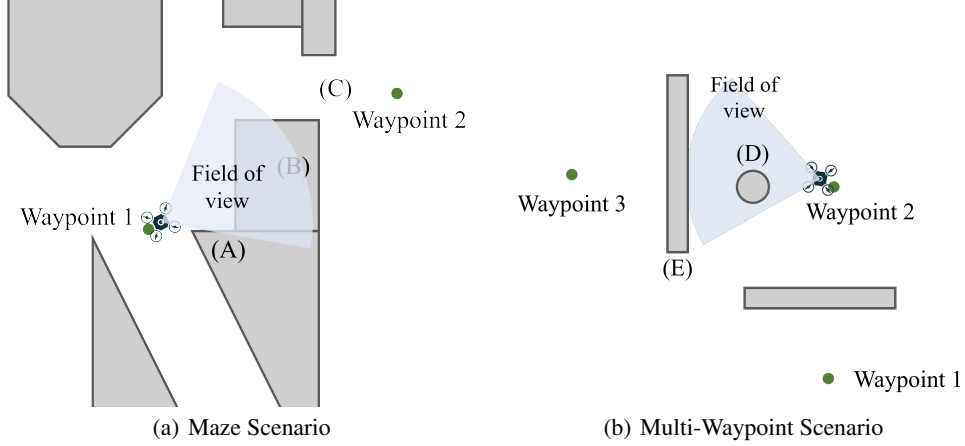


Figure 6: Visualization of failure cases.

C.3 Analyses on Effectiveness of Different Metrics

Correlation Calculation Method. As the value of two metrics to be calculated for the correlation coefficient are denoted as $\{x_i\}$, $\{y_i\}$, respectively. The correlation coefficient between $\{x_i\}$ and $\{y_i\}$ defines as

$$\text{Corr}_{x,y} = \frac{\sum_i (x_i - \bar{x})(y_i - \bar{y})}{\sqrt{\sum_i (x_i - \bar{x})^2 \sum_i (y_i - \bar{y})^2}}, \quad (4)$$

where \bar{x} , \bar{y} are the average values of $\{x_i\}$ and $\{y_i\}$.

Results. Fig. 7 shows the correlation coefficients between six performance metrics and three difficulty metrics for each method across multiple scenarios. As analyzed in Sec. 4.3, TO and AOL significantly impact the motion performance of two privileged planners (Fig. 7(a) and Fig. 7(b)). In scenarios with high TO and AOL, the planners tend to fly slower, consume more energy, and exhibit less smoothness. Ego-vision methods are notably influenced by partial perception, making VO a crucial factor. Consequently, high VO greatly decreases the success rate of ego-vision methods, much more so than it does for privileged methods.

When comparing the computation times of different methods, we observe that the time required by learning-based methods primarily depends on the network architecture and is minimally influenced by the scenario. Conversely, the computation times for optimization- and sampling-based methods are affected by both AOL and TO. Scenarios with higher TO and AOL demonstrate increased planning complexity, resulting in longer computation times.

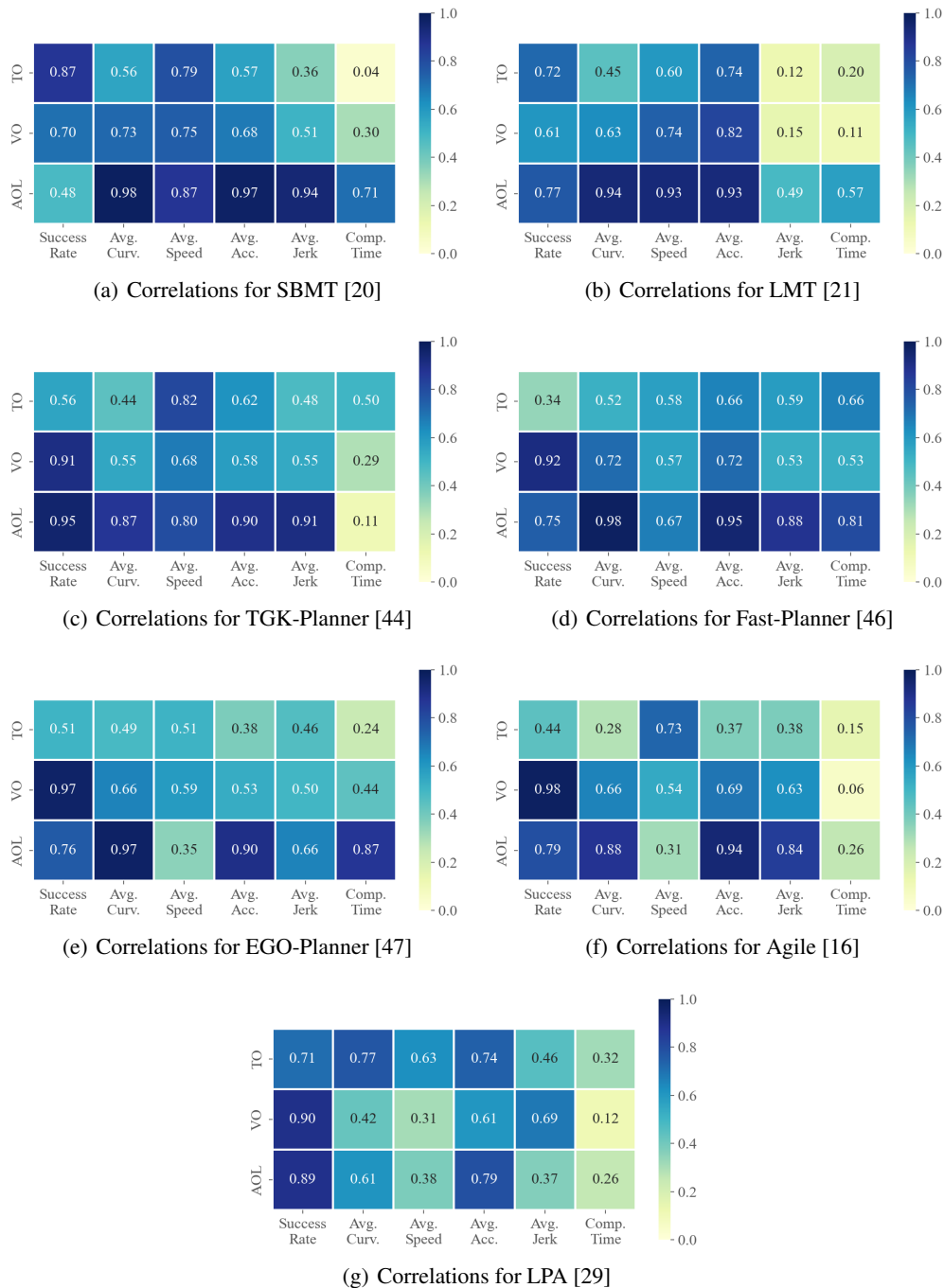


Figure 7: Correlation coefficients between three difficulty metrics and evaluation metrics for each method.